Inspection of 3D parts using high accuracy range data

F. Prieto[a,b], R. Lepage[b], P. Boulanger[c] and T. Redarce[a]

[a]INSA, Laboratoire d'Automatique Industrielle
20 avenue Albert Einstein 69621 Villeurbanne Cedex France

[b]ÉTS, Laboratoire d'Imagerie, de Vision et d'Intelligence Artificielle
1100 rue Notre-Dame Ouest Montréal, Québec, H3C 1K3 Canada

[c]NRCC, Institute for Information Technology
Montreal road, building M-50 Ottawa, Ontario, K1A 0R6 Canada

ABSTRACT

The use of a laser range sensor in the 3D part digitalization process for inspection tasks allows very significant improvement in acquisition speed and in 3D measurement points density but does not equal the accuracy obtained with a coordinate measuring machine (CMM). Inspection consists in verifying the accuracy of a part related to a given set of tolerances. It is thus necessary that the 3D measurements be accurate. In the 3D capture of a part, several sources of error can alter the measured values. So, we have to find and model the most influent parameters affecting the accuracy of the range sensor in the digitalization process. This model is used to produce a sensing plan to acquire completely and accurately the geometry of a part. The sensing plan is composed of the set of viewpoints which defines the exact position and orientation of the camera relative to the part. The 3D cloud obtained from the sensing plan is registered with the CAD model of the part and then segmented according to the different surfaces. Segmentation results are used to check tolerances of the part. By using the noise model, we introduce a dispersion value for each 3D point acquired according to the sensing plan. This value of dispersion is shown as a weight factor in the inspection results.

Keywords: Inspection, 3D scanning, CAD-based vision, segmentation

1. INTRODUCTION

CAD/CAM is largely used in industry. After the design of the object and the manufacturing of the part remains a significant task: the *inspection*. Inspection is the process of determining if a product (part or object) deviates from a given set of specifications (tolerances). Coordinate Measuring Machine (CMM) is the industry standard mechanism for part validation, but in spite of its high accuracy, it has some important limitations such as: the need for mechanical fixturing, low measurement speed and the need to be programmed as new part is inspected.

On the other hand, recent advances in non-contact sensor like laser range finder, with significant improvement in speed (about 20000 points/s), allow them to be used in inspection tasks. The disadvantage of the range sensors is their accuracy, largely lower than the CMM accuracy. If one wants to improve this accuracy, it is necessary to develop acquisition strategies that optimize the digitalization process in order to improve the accuracy. Finally, if the dimensional inspection is relatively simple to realize, it is necessary however to develop methodologies for geometrical inspection.

In this paper we present an inspection methodology for geometrical tolerances that uses the CAD model of the part and a high accuracy 3D range data obtained after the scanning of the 3D part using an acquisition strategy that optimizes the accuracy.

The 3D range camera and its noise model is presented in Section 2. The 3D data acquisition strategy is briefly discussed in Section 3. Section 4 describes the inspection methodology. Results are presented in Section 5.

Other author information:
FP, TR: Email: {fprieto, redarce}@lai.insa-lyon.fr
R. L.: Email: lepage@livia.etsmtl.ca
P. B.: Email: boulanger@iit.nrc.ca

2. THE 3D RANGE CAMERA

This section describes the optical principle of the range camera used and the accuracy of the 3D data as a function of the camera placement. The camera, an auto-synchronized range sensor, was developed at National Research Council of Canada[1].

In order to evaluate the accuracy of the cloud of 3D points obtained by the scanning process, we have achieved 128 measurements in different positions for distance and orientation of the laser sensor with respect to a reference surface. The measurements were fulfilled after the camera calibration process, and the camera placements were near to calibration ones.

In Figure 1(a), we show the variance (in mm^2) in the axis of the projected beam versus the distance (in mm) from the camera to the surface. The dotted curve is a second degree polynomial that best fit the real variances curve. The fitting curve is defined by $Var(d) = 8.86 \times 10^{-10} \cdot d^2 - 3.47 \times 10^{-7} \cdot d + 3.81 \times 10^{-5}$. From Figure 1(a), we can conclude that in spite of oscillations, the variance has a smaller dispersion when the camera is the nearest to the surface. To improve the measurement accuracy by finding the best scanning placements, we define a distance range for the placements as $170mm \leq d \leq 240mm$.

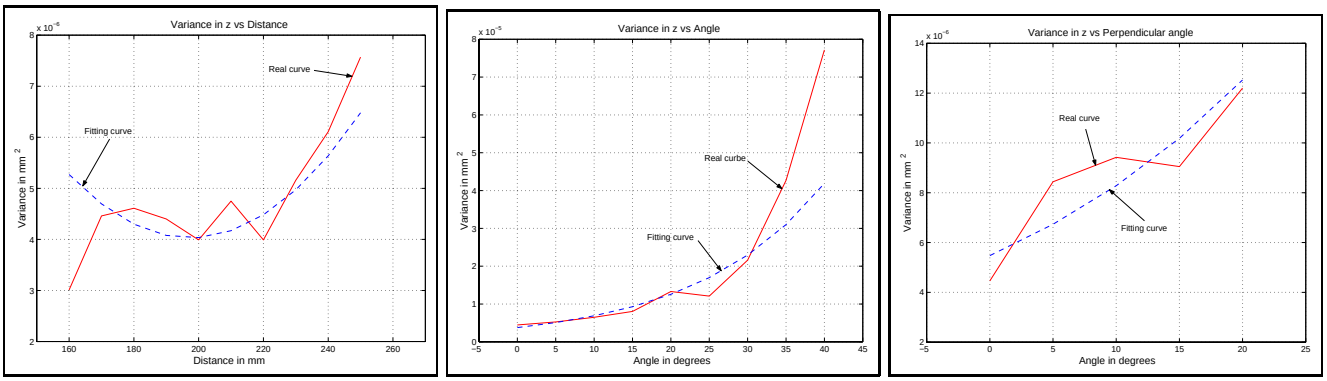

(a) Variance in Z versus distance.

(b) Variance in Z versus incident angle in the direction of the laser sweep.

(c) Variance in Z versus incident angle in a perpendicular direction to the laser sweep.

Figure 1. Variance of the range sensor in the Z direction.

In Figure 1(b), we show the variance (in mm^2) in the laser propagation axis versus the incident angle (in degrees) the laser beam reaches the surface. The dotted curve is an exponential function $Var(\alpha) = 3.77 \times 10^{-6} \cdot e^{6.01 \times 10^{-2} \cdot |\alpha|}$ that best fit the real curve of variances. The incident angle is measured in the same direction as the laser beam sweep. From Figure 1(c), we observed that the smaller value of dispersion is produced for an incident angle near to zero degrees, or normal to the surface. For the definition of the best scanning placements, we set the laser beam sweep range as $-35° \leq \alpha \leq 35°$. The range starts at $-35°$ and not $0°$ because we have a symmetrical result when the angle α increases in the opposite direction.

Another parameter which influences the value of the variance is the incident angle in a perpendicular direction from the laser beam sweep (angle (β)). In Figure 1(c), we present the variance (in mm^2) in the axis of the beam projection versus the incident angle β (in degrees). The dotted curve is an exponential function $Var(\alpha) = 5.47 \times 10^{-6} \cdot e^{4.15 \times 10^{-2} \cdot |\beta|}$, the best fit of the real variance curve. Similarly to the angle α, we can conclude from Figure 1(c) that the dispersion is smaller when the incident angle is near to zero, or normal to the surface. For the definition of the best scanning placements, and looking at the behavior of the curve, we have set the laser beam sweep range as $-15° \leq \beta \leq 15°$.

These results confirm that we can improve the accuracy of the data acquisition process by following the previously defined criterions (normal direction, distance). So, in order to be able to achieve inspection tasks, we have

implemented an acquisition planning strategy. The strategy improves the 3D data accuracy by finding the optimal camera placement for digitizing the part, using the range of the parameters d, α and β computed in this section.

3. AN OPTIMUM 3D DATA ACQUISITION STRATEGY

The main goal of this strategy is to improve the measurement accuracy of a part. Such a strategy consists in computing the set X of viewpoints x^i in order to obtain a complete and optimal 3D image of the part. We define an optimal 3D image as a 3D cloud acquired by the scanning process in the best accuracy conditions. The resulting 3D image can be used, for instance, in inspection task for verifying the specification of just a few surfaces. Our strategy is therefore to find the collection of viewpoints for each surface independently. If one wants to digitize the whole part, he just has to add the complete assemblies X of all the surfaces in the part. In most of the related works[2–4], the acquisition strategy is optimized to have the minimum number of viewpoints to digitize the whole part. In our work[5], the placement strategy optimizes the accuracy of the acquired 3D points and can be applied to a particular surface or to the whole part.

We define a viewpoint as a set of 7 parameters $x^i = \{x, y, z, \phi, \theta, \psi, \gamma\}^i$, with three position parameters (x, y, z) defining the spatial placement of the camera relative to the coordinate system of the part, three orientation parameters (ϕ, θ, ψ) defining the direction of the laser beam, and one parameter γ specifying the angle of the controlled sweep. Figure 2 shows a viewpoint with all its parameters. We do not consider optical parameters because the laser camera is previously calibrated. The set X of viewpoints x^i is defined $X = \{x^1 x^2 ... x^i ... x^n\}$, with n the minimum number of viewpoints to digitize a simple surface or the whole part.

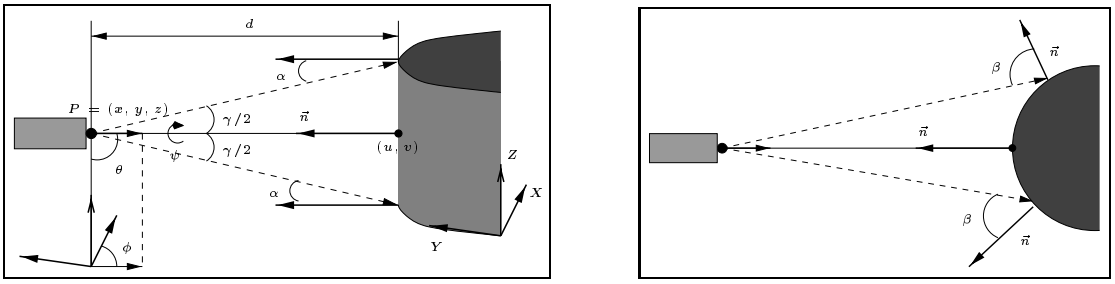

(a) Front view.

(b) Top view.

Figure 2. Viewpoint parameters.

The system requirements are: knowledge of the exact position and orientation of the part and of the CAD model of the part in IGES format. We use a registration process to determine the placement of the part, as implemented by Moron[6], which relies on the work of Besl and McKay[7]. This process registers an unordered cloud of 3D points of the part with its CAD model. The CAD model is used not only for the registration process, but also for the search of viewpoints and to resolve the occlusion problem.

From the last section, we showed that the accuracy of a measured point using an auto-synchronized range sensor (previously calibrated) depends specifically on the scanning distance and on the incidence angle of the laser beam relative to the surface. We have found for the auto-synchronized range sensor that the near and far field view planes are $170mm$ and $240mm$ respectively. The measured points are therefore more accurate when the camera is located near the part. For the best accuracy, the ideal incident angle the laser beam reaches the surface is 90 degrees ($\alpha = 0$ and $\beta = 0$ see Figure 2), that is the more the angle of incidence of the laser ray is near to the normal direction of the surface, the more the measured points are accurate. Our strategy searches for viewpoints to digitize the part with the best conditions for accuracy.

The viewpoint issue of our strategy is that inspected surface can be reached by the camera mechanical support and is occlusion free. A surface is occluded for a specific viewpoint if any object intersects the laser beam before reaching the target surface. The system works with both simple and complex surfaces. The only geometric constraint imposed to the parts to be digitized is that they are completely contained in the workspace of the camera.

The algorithm's pseudocode implemented as a solution to this problem is:

3D data acquisition strategy algorithm

1. Input data.
  1.1. Extract data from the CAD model.
  1.2. Generate the 3D voxel model.
2. Find the viewpoints set.
  2.1. Project viewpoints on the surface.
  2.2. Find the optimal viewpoint placement.
  2.3. Verify the reachability and the non-occlusion conditions.
3. Estimate 3D data accuracy.

3.1. Input data

Two processes basically generate the input data required for the algorithm. A first process extracts from the CAD file the needed data to search for viewpoint on the surfaces. The second process generates a 3D voxel model of the part.

CAD model. A CAD model of the part in IGES format is input to the algorithm. The IGES file contains the exact representation of the part using NURBS (Non-Uniform Rational B-Splines) surfaces parameters.

3D voxel model. If we extend the concept of a two-dimensional binary bitmap, where each pixel (r, s) can take just one of two values, each voxel (i, j, k) in the 3D space can take one of two values: 0 (unoccupied) or 1 (occupied). An occupied voxel contains some portion of any of the surfaces that make up the part. The *3D voxel model* is the addition of all occupied voxels.

3.2. Search for the viewpoints set

Tthe NURBS surface parameters from the CAD model are used to search the viewpoints and to solve the occlusion and collision problem. We first generate a 2D bitmap of each surface to find the viewpoints projection on the surface. Then, the optimal placement for the viewpoint is computed using the normal direction of the surface to each projected viewpoint. Finally, the occlusion and collision problems are solved by using the *3D voxel model*.

Viewpoints projection on the surface. We look for the set of projected viewpoints that define the trajectory that the camera mechanical support (a CMM in this work) has to follow in order to digitize the whole surface. The laser sweeping ray orientation has to be perpendicular to this trajectory to guarantee the minimal sweep distance from the trajectory to the edges of the surface.

Optimal viewpoint placement. To complete the definition of a viewpoint, we need to find its position and orientation in space. For that purpose, we minimize the dispersion from the noise model obtained in Section 2.

Reachability and the non-occlusion solutions. The next step in our strategy is to verify that the viewpoint position is reachable and is free from occlusion problem. For the reachability issue, we suppose that the part is in the center of a sphere, and that the viewpoints out of this sphere can be reached by the mechanical support of the camera. For the verification of occlusion conditions, we insure that any object does not intersect the laser beam coming from the viewpoint position to the target surface. When an occlusion problem is detected, the system seeks for a new viewpoint by moving the old viewpoint in the parametric directions of the surface. The new viewpoint will remain as near as possible to the normal direction to optimize the accuracy, but ensures the visibility of the region to be digitized.

3.3. Estimation of 3D data accuracy

Once all the viewpoints have been located, satisfying non-occlusion conditions, the strategy computes the accuracy of the 3D measured points as obtained from this set of viewpoints. If the result is satisfactory, this means that the 3D measured points have a better or the same accuracy as the specified one, and then the solution is retained. Otherwise, a new set of viewpoints must be defined, and the algorithm is repeated from step 2: *Find the viewpoints set X*.

The accuracy of measured points in the case of an auto-synchronized camera is a function of the distance d between the camera and the part being digitized and the incident angles α and β of the laser beam. Thus, to estimate the accuracy of measured points, we must compute these parameters. Figure 3 illustrates some special configurations for the determination of α and β parameters. The parameter d has been defined in a previous algorithm step.

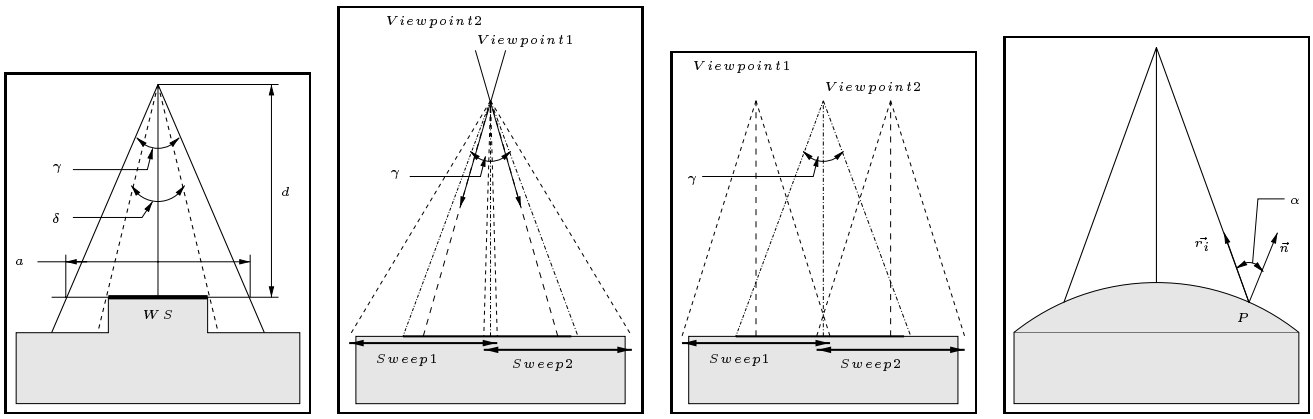

(a) For a field of view greater than the surface.

(b) Changing the viewpoint orientation to digitize the whole width of the surface.

(c) Defining 2 new viewpoints to digitize the whole width of the surface.

(d) Estimation on a complex surface.

Figure 3. Evaluation of α and β parameters.

Figure 3(a) illustrates the case where the field of view of the range sensor is greater than the width of the surface to be measured. The amplitude of the sweeping ray is computed from the field of view γ and the distance d. The width of the surface WS is obtained from the CAD model. As the resolution of the camera is well-known, that is the number of points in a sweep, the angle δ is calculated and so the incident angle of the sweep portion hitting the surface.

When the width of the measured surface is greater than the field of view of the range sensor, the strategy modifies the orientation of the camera (by using the mechanical support) in such a way that the incident angles α is always $-35° \leq \alpha \leq 35°$ range (see Figure 3(b)). If the maximum α value is reached and the width of the surface has not been completely digitized, the trajectory is divided into two parallel trajectories as shown in Figure 3(c). These computations are repeated iteratively until the whole surface is digitized.

In Figure 3(d) we present the computation of the incident angle α in a curved surface. The point P where the ray touches the surface is computed by using the 3D surface model. The normal on the surface at this point is obtained from the parametric NURBS surface. Finally the angle α is computed by developing the inner product of two vectors $\vec{r_i} \cdot \vec{n}$. When the surface is curved in the two parametric directions (u and v), the incident angles α and β are computed using the components of the normal in the direction of α and β variations.

Once the parameters d, α and β are known, the accuracy is computed as the sum of the dispersions introduced by each parameter, and obtained from the models developed in Section 2.

4. TOLERANCE INSPECTION

Manufacturing methods are unable to produce parts with perfect shapes, sizes and forms. Therefore, given a physical instance of a part, it is possible to measure dimensional or geometric properties, and determine if deviations are within bounds defined by the tolerance specification. In this section, we will define a few of the tolerance types and give explanation of the algorithms to make those tolerance measurements on an object feature.

Usually the inspection of a part using 3D range data is done by comparing the CAD model with this 3D data after registration[8,9,4]. In order to use only the 3D points related to the tolerance specification (points on the reference surface and points on the inspected surface), the 3D cloud is segmented after the registration process[10,11].

A *datum* is a geometric surface from which dimensions are measured when so specified or to which geometric tolerances are referenced. It has an exact form and represents an accurate or fixed location, for purposes of manufacturing or measurement. A *datum feature* is a feature of a part, such as a surface, which forms the basis for a datum or is used to establish its location. We will use datums as obtained from the CAD model (IGES format) of the part. As a datum feature, we use the segmented set of 3D measured points related to the datum.

4.1. The registration method

The registration of two shapes is defined as finding the 3D rigid transformation (rotation + translation) to be applied on one of the shape to bring it into one common cartesian coordinate system with the other one. The registration process relies on the well-known work of Besl and McKay[7] who in 1992 developed a general-purpose representation method for the accurate and computationally efficient registration of 3D shapes, including free-form curves and surfaces. The method is based on the Iterative Closest Point (ICP) algorithm, which requires only to find the closest point from a geometric entity to a given point. The rigid transformation is computed using a unit quaternion. But as the transformation estimate is done by a Mean Square (MS) distance computation, this method is not robust to outliners points, generated either by noise or by the presence of other parts in the scene.

As a solution to this problem, Masuda and Yokoya[12] estimate the rigid motion between two range images in a robust way by fusing the ICP algorithm with random sampling and Least Median of Squares (LMS) estimation. They demonstrated that registration between two images can be achieved with a high level of robustness (up to 50 %) to occlusion and noise.

Moron[13] implemented an algorithm for registration between an unordered cloud of 3D points and a CAD model in STL or IGES format. In the registration process, Moron use the CAD model in STL format rather than in IGES format, so that few precision is lost but computation time is largely improved.

4.2. The segmentation method

In the registration process, we superposed the CAD model with the 3D data of the part. But because we are interested in inspecting some specific surfaces, we need to segment the part into its different surfaces. The segmentation of the 3D cloud is done by computing the distance between every 3D point and all of the surfaces in the CAD model (IGES format), and by comparing some local geometric properties between each 3D point in the cloud and its closest point on the surface. In the IGES CAD model, all the surfaces of the part are defined as a parametric NURBS (Non-Uniform Rational B-Splines) surfaces.

4.2.1. Point/NURBS surface distance computation

The distance of a 3D point to a NURBS surface can be computed as follow: find a point on the parametric space of the surface (u_0, v_0) such that the distance between the surface $\vec{s}(u_0, v_0)$ and the point $\vec{r}$ is minimum in a direction perpendicular to the tangent plane at the point. The function to be minimized is the following:

$$min_{u_0,v_0} \|\vec{r} - \vec{s}(u,v)\|^2.$$

If one performs the Taylor expansion of the parametric surface $\vec{s}(u,v)$, we obtain:

$$\vec{s}(u,v) = \vec{s}(u_0,v_0) + \frac{\partial \vec{s}}{\partial u}(u_0 - u) + \frac{\partial \vec{s}}{\partial v}(v_0 - v).$$

Using this expansion, the minimization problem becomes:

$$min_{u_0,v_0} \|\vec{r} - \vec{s}(u_0,v_0) - \frac{\partial \vec{s}}{\partial u}(u_0 - u) - \frac{\partial \vec{s}}{\partial v}(v_0 - v)\|^2.$$

This can be expressed in matrix form as:

$$min_{u_0,v_0} \|J\vec{w} - \vec{d}\|^2$$

where J is the Jacobien matrix of $\vec{s}(u,v)$ and $\vec{w}$ is equal to the variation of the parametrization.

$\vec{d}(u,v)$ is the error for the initial parametrization (u_t, v_t), i.e. the initial closest point to the CAD format, so $\vec{d}(u,v) = \vec{r} - \vec{s}(u,v)$. Then the solution to the minimization problem is equal to: $\vec{w} = (J^T J)^{-1} J^T \vec{d}$. Using an iterative procedure, one can compute the distance of the point from the surface in less than four to five iterations.

4.2.2. Geometric properties comparison

Let P be a point from the 3D range data, and Q the closest point to P on the surface. To terminate the segmentation process, we estimate and compare some local geometric properties of P and Q. Geometric properties of Q are estimated using the NURBS CAD model. We estimate the local geometric properties of P by using the method proposed by Boulanger[14]. This method is viewpoint invariant because the surface estimation process minimizes the distance between the surface NURBS surface $\vec{s}$ and the 3D data point in a direction perpendicular to the tangent plane of the surface at this point. Finally, we compare the local geometric properties of Q, estimated from the NURBS surface, to P from the 3D range data. Let α_{tol} be the permissible angle between the surface normal $\vec{N}_s$ and 3D data normal $\vec{N}_r$ at point P. Then the condition $|Angle(\vec{N}_s, \vec{N}_r)| \leq \alpha_{tol}$ has to be respected. Let K_{tol} and H_{tol} be the defined variation of the gaussian and the mean curvatures, then the conditions: $|K_s - K_r| \leq K_{tol}$ and $|H_s - H_r| \leq H_{tol}$ have to be respected.

4.3. Geometrical tolerance

The geometrical tolerance is the maximum interval acceptable in which can vary the geometrical characteristics of form, orientation or position of an element.

Figure 4 shows the tolerance specifications (in mm) of a part. As this information is not present in the CAD model, we have to add it in an independent file.

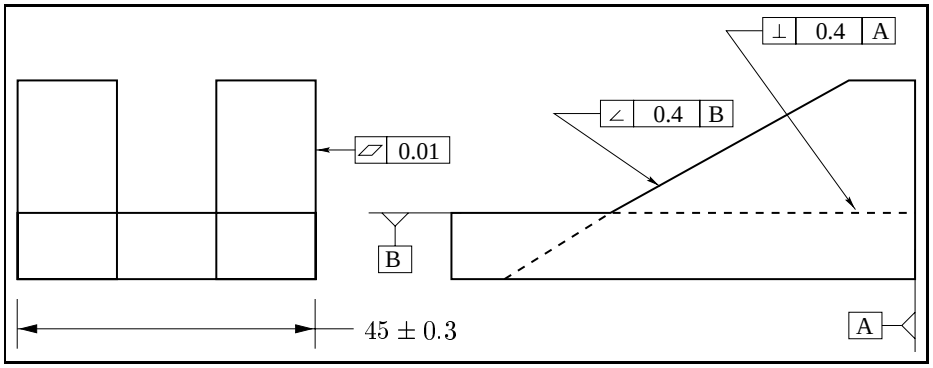

Figure 4. Tolerance specifications

4.3.1. Form tolerance

This is the maximum deviation allowed to the form of an element. According to the geometry of the element, the zone of tolerance is limited by two surfaces, distant of t_s and between which must be located the surface considered. A form tolerance applies only to the shape of the toleranced element independently of its environment, its position or its orientation. Flatness, straighness, cylindricity and profile of a surface are some of the form tolerances.

We check form tolerances of a surface by using only the 3D points associated with this surface and obtained from the segmentation process. This subset of 3D points is registered with the CAD model, and the perpendicular distance between each 3D point and the NURBS surfaces is calculated. The distribution of these distances is used to define the zone of measured tolerance. Indeed, we adjust the average value of the distribution with the NURBS surface (of the CAD model). We place two parallel surfaces to the NURBS surface at a distance $\pm 2\sigma$, then the measured tolerance is equal to: $t_m = 4\sigma$.

For form tolerances, we say that surface is in conformity with the specification if the following relation is satisfied:

$$t_m \leq t_s, \tag{1}$$

where: t_m is the measured distance between the parallel plans and t_s is the specified tolerance.

4.3.2. Orientation tolerance

It is the maximum deviation allowed for the orientation of an element related to an element of reference. The zone of tolerance is limited by two planes or a cylinder inside of which must be located the surface considered. The zone of tolerance is mobil in translation and does not determine nor control the position of the element. Angularity, perpendicularity and parallelism are examples of orientation tolerances.

In order to verify the conformity of an orientation tolerance, we must use two subsets of points: S_i associated to the surface to be inspected and S_r associated to the reference surface. The subset S_r is registered with CAD model and the computed rigid transformation is also applied to S_i. The perpendicular distance between each 3D point of S_i and NURBS surface is calculated. The distribution of these distances does not have a gaussian form, and thus two points are defined in order to evaluate the zone of measured tolerance: the point p_1 at a distance d_1 from the NURBS surface such that 2.5% of the points in S_i have a distance $d_i \leq d_1$, and the point p_2 at a distance d_2 from the NURBS surface such that 2.5% of the points in S_i have a distance $d_i \geq d_2$. The zone of measured tolerance is then defined as the range between two parallel planes with an orientation related to the reference surface and passing through the points p_1 and p_2. For orientation tolerances, the inspected surface is in conformity with the specification t_s if the following relation is satisfied:

$$t_m = |d_2 - d_1| \leq t_s. \tag{2}$$

4.3.3. Location tolerance

This is the maximum deviation allowed for the location of an element. The zone of tolerance is limited by two planes, a parallelepiped or a cylinder inside of which must be located the surface considered. The zone of tolerance must be directed and located according to one or more elements of reference.

The location tolerances are controlled similarly to the tolerances of orientation. To ensure the conformity of the surface under inspection, the following relation must be satisfied:

$$t_{1_s} \leq t_{1_m} < t_{2_m} \leq t_{2_s}, \tag{3}$$

where: t_{1_s} and t_{2_s} are the distances from the surfaces which define the zone of tolerance specified to the reference, and t_{1_m} and t_{2_m} are the distances from the surfaces which define the zone of tolerance measured to the real reference (S_r).

4.4. Nondeterministic inspection

A real image is seldom free from noise, and thus leads to uncertainties in the attributes of the entities resulting from image processing. In the case of 3D images, these entities are the subsets of 3D points (after the segmentation process) and the 3D points themselves. Uncertainty in the entities of the image leads to uncertainty in the inspection tasks. In this section we discuss the effect of this uncertainty in the results of the inspection. We suppose that the range data was obtained by using a strategy detailed in section 3.

4.4.1. Noise model

We have exposed in section 2 the noise model of the digitalization system. Let $\vec{r}_{ij}$ be the real value of the point (x_i, z_j) on surface, and let $(\hat{x}_i, \hat{z}_j)$ be the acquired value of the point The model for a noisy point measured by the sensor is: $(\hat{x}_i, \hat{z}_j) = (x_i, z_j) + b(x_i, z_j)$.

The noise is described by a probability density function with a gaussian distribution of mean zero and variace σ, as follow:

$$b(\vec{r}) = \frac{1}{(2\pi)^{3/2}\sqrt{|\Sigma|}} exp\left(-\frac{1}{2}(\vec{r}-\vec{s})^\top \Sigma^{-1}(\vec{r}-\vec{s})\right), \tag{4}$$

where $\vec{s}$ is a two-dimensional vector corresponding to the point on the NURBS surface nearest to $\vec{r}$, and $\Sigma(\vec{r})$ is the covariance matrix for the point $\vec{r}$.

The properties of the noise function $b(\vec{r})$ can be interpreted geometrically, assigning a constant probability to the intersection of the function $b(\vec{r})$ with an horizontal plane. These intersections form a family of ellipses. When

the center of the ellipse coincides with the origin of the reference frame, the form and the orientation are defined completely by Σ. Indeed, the length of the major and minor axes can be calculated easily as the square root of the eigenvalues of Σ. The length of the axes of the dispersion ellipse for the point $\vec{r}$ can then be calculated:

$$L_x(\vec{r}) = \sqrt{\frac{1}{2}(\sigma_{xx}(\vec{r}) + \sigma_{xz}(\vec{r}))}, \qquad L_z(\vec{r}) = \sqrt{\frac{1}{2}(\sigma_{xz}(\vec{r}) + \sigma_{zz}(\vec{r}))}, \tag{5}$$

where $L_x(\vec{r})$ is the length of the minor axis and $L_z(\vec{r})$ is the length of the major axis, since for the point $\vec{r}$ we know that $\sigma_{zz}(\vec{r}) > \sigma_{xz}(\vec{r})$ (Section 2).

4.4.2. Noise consideration in inspection results

The matrix of covariance Σ is a function of the digitalization parameters such as: the incident angle α from the laser beam on the surface in the direction of the laser sweep, the incident angle β from the laser beam on the surface in a perpendicular direction to the laser sweep and the distance d from the sensor to the surface.

The form of the variance at the point $\vec{r}$ is an ellipse, the major axis showing the largest dispersion of the point $\vec{r}$. We compute the major axis (equation 5) using $\sigma_{xz}(\vec{r})$ and $\sigma_{zz}(\vec{r})$ computed in Section 2:

$$\begin{aligned} \sigma_{xz}(\alpha) &= 6.47 \times 10^{-7} \cdot e^{5.91 \times 10^{-2} \cdot |\alpha|}, \\ \sigma_{xz}(\beta) &= 8.30 \times 10^{-7} \cdot e^{4.40 \times 10^{-2} \cdot |\beta|}, \\ \sigma_{xz}(d) &= 9.92 \times 10^{-11} \cdot d^2 - 3.82 \times 10^{-8} \cdot d + 4.34 \times 10^{-6}, \end{aligned} \tag{6}$$

for $\sigma_{xz}(\vec{r}) = \sigma_{xz}(\alpha) + \sigma_{xz}(\beta) + \sigma_{xz}(d)$, and:

$$\begin{aligned} \sigma_{zz}(\alpha) &= 3.77 \times 10^{-6} \cdot e^{6.01 \times 10^{-2} \cdot |\alpha|}, \\ \sigma_{zz}(\beta) &= 5.47 \times 10^{-6} \cdot e^{4.15 \times 10^{-2} \cdot |\beta|}, \\ \sigma_{zz}(d) &= 8.86 \times 10^{-10} \cdot d^2 - 3.47 \times 10^{-7} \cdot d + 3.81 \times 10^{-5}, \end{aligned} \tag{7}$$

for $\sigma_{zz}(\vec{r}) = \sigma_{zz}(\alpha) + \sigma_{zz}(\beta) + \sigma_{zz}(d)$.

Let $L_{z\ min}$ be the minimum value of L_z obtained in optimal digitalization conditions, thus: $\alpha = 0°$, $\beta = 0°$ and $d = 170mm$. Let $L_{z\ ,max}$ be the maximum value of L_z obtained in extreme digitalization conditions, thus: $|\alpha| = 35°$, $|\beta| = 15°$ and $d = 240mm$.

We define the mean value of dispersion of a 3D cloud as:

$$\bar{L}_z = \frac{1}{n} \sum_{i=1}^{n} L_z(\vec{r}_i), \tag{8}$$

with n the number of 3D points in the cloud.

Let t_s be a specified tolerance and t_m the measured deviation of a part under inspection. The deterministic inspection dictates that the part is in conformity with the specification if $t_m \leq t_s$. In nondeterministic inspection the result of the inspection must take into account the dispersion of the points used to carry out the tolerance control. We illustrate in Figure 5 the possible regions t_m can take in relation to t_s.

The location of t_m related to t_s is used to quantify the result of the tolerance inspection by a qualitative value of reliability. In the next table we summarize the quantization of the inspection results according to the possible regions.

The quantizations *enough reliable* and *unreliable* indicates that the inspection system is not sufficiently accurate to control the specified tolerance. Therefore it would be necessary either to improve the precision of the 3D data (to reduce $\bar{L}_z$ as much as possible), or to use another method of inspection.

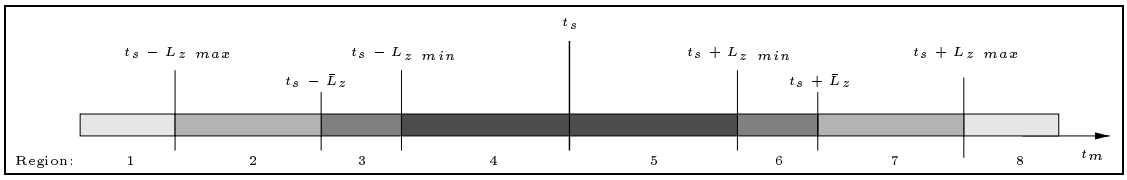

Figure 5. Location of t_m related to t_s

Table 1. Quantization of the nondeterministic inspection result

Region	Location of t_m related to t_s	Inspection result	Reliability value
1	$t_m < t_s - L_{z\ max}$	Tolerance conform	very highly reliable
2	$t_s - L_{z\ max} \leq t_m < t_s - \bar{L}_z$	Tolerance conform	highly reliable
3	$t_s - \bar{L}_z \leq t_m < t_s - L_{z\ min}$	Tolerance conform	enough reliable
4	$t_s - L_{z\ min} \leq t_m < t_s$	Tolerance conform	unreliable
5	$t_s \leq t_m < t_s + L_{z\ min}$	Tolerance not conform	unreliable
6	$t_s + L_{z\ min} \leq t_m < t_s + \bar{L}_z$	Tolerance not conform	enough reliable
7	$t_s + \bar{L}_z \leq t_m < t_s + L_{z\ max}$	Tolerance not conform	highly reliable
8	$t_s + L_{z\ max} \leq t_m$	Tolerance not conform	very highly reliable

5. INSPECTION RESULTS

5.1. Standard inspection results

We intend to check the specified tolerances in Figure 4. In order to know the exact deviations of these tolerances, we carried out the control with a CMM whom accuracy is $5\mu m$. We show the results in Table 2 with the tolerance under control, the value of specified tolerance (t_s), the measured value (t_m) and the result of the inspection.

Table 2. Tolerances inspection using the CMM

Tolerance name	Tolerance specification	Measured value	Result
Size tolerance	$45 \pm 0.3\ mm$	$45.016 \pm 0.001\ mm$	Conform
Flatness	$10\mu m$	$10.8\mu m$	Not conform
Perpendicularity	$400\mu m$	$39\mu m$	Conform
Angularity	$400\mu m$	$26\mu m$	Conform

Inspection using 3D data coming from a standard digitalization process The inspection results using the 3D cloud coming from a standard digitalization process are gathered in Table 3. We obtain similar inspection results to those obtained with the CMM, but the column of the measured tolerance shows that these values are less precise than those obtained with the CMM.

Inspection using 3D data coming from a digitalization process with the acquisition strategy We show in Table 4 the results of the tolerance inspection using the 3D data coming from a digitalization process with the acquisition strategy. The inspection results obtained are identical to the previous case (standard digitalization process), but the values of the measured tolerances are smaller, thus converging toward the inspection with the CMM.

We conclude that the capacity to control tolerances does not depend exclusively on the type of range sensor used, but also in the way in which the digitalization of the part is done. The choice of scanning process to be used depends on the values of tolerances we wish to control. To control tolerances near $75\mu m$, a standard numerisation is sufficient and for the control of tolerances near $50\mu m$ the use of the acquisition strategy is necessary.

Table 3. Tolerance inspection using the 3D data coming from a standard digitalization process

Tolerance name	Tolerance specification	Measured value	Result
Size tolerance	$45 \pm 0.3\ mm$	$44.993 \pm 0.038\ mm$	Conform
Flatness	$10\mu m$	$72\mu m$	Not conform
Perpendicularity	$400\mu m$	$134\mu m$	Conform
Angularity	$400\mu m$	$41\mu m$	Conform

Table 4. Tolerance inspection using 3D data coming from a digitalization process with the acquisition strategy

Tolerance name	Tolerance specification	Measured value	Result
Size tolerance	$45 \pm 0.3\ mm$	$44.999 \pm 0.012\ mm$	Conform
Flatness	$10\mu m$	$13\mu m$	Not conform
Perpendicularity	$400\mu m$	$93\mu m$	Conform
Angularity	$400\mu m$	$34\mu m$	Conform

5.2. Nondeterministic inspection results

Using the acquisition strategy for the digitalization process we know the α, β and d parameters and therefore we can compute $L_{z\ min}, L_{z\ max}$ and $\bar{L}_z$ and perform nondeterministic inspection (as presented in Section 4.4). Table 5 shows nondeterministic inspection results.

The size tolerance as well as the geometrical tolerances of perpendicularity and angularity were found in conformity with the specifications, with a reliability value scoring *very highly reliable*. The geometrical tolerance of flatness was found not-conform with the specification, with a reliability score *unreliable*. The reliability value *unreliable* is due to the small value of the specification ($10\mu m$), and consequently another method of tolerance inspection should be used.

Table 5. Nondeterministic tolerance inspection

Tolerance name	Result	Reliability value
Size tolerance	Conform	Very highly reliable
Flatness	Not conform	unreliable
Perpendicularity	Conform	Very highly reliable
Angularity	Conform	Very highly reliable

6. CONCLUSION

We have presented an inspection system for manufactured parts that uses high accuracy range data. The high accuracy range data is obtained by using an optimum 3D data acquisition strategy.

We have defined and implemented a methodology to check geometric tolerances, using a cloud of 3D points and a CAD model of the part. The system first registers a cloud of 3D points with a CAD model of the part, and then segments the 3D points in different surfaces by using the IGES CAD model. From the CAD model we know the exact description of the part, so we can use this methodology to make the inspection of parts with complex surfaces.

The results presented in this work show that the precision of the 3D data obtained with a range sensor is improved by the use of an acquisition strategy. These high precision 3D data are particularly interesting when very fine inspection is required. The acquisition strategy allows us to introduce a reliability value to the inspection result, and thus carries out a nondeterminist inspection. This reliability value constitutes a decision-making aid for the acceptance or rejection of the part under control.

REFERENCES

1. F. Blais, M. Rioux and J.A. Beraldin, "Practical considerations for a design of a high precision 3-D laser scenner system," in *SPIE Optomechanical and Electro-Optical Design of Industrial Systems*, pp. 225–246, (Bellinghan), June 1988.
2. G.H. Tarbox and S.N. Gottschlich, "Planning for complete sensor coverage in inspection," *Computer Vision and Image Understanding* **61**, pp. 84–111, January 1995.
3. K.A. Tarabanis, R.Y. TSAI and K. ANIL, "Computing occlusion-free viewpoints," *IEEE Transactions on Pattern Analysis and Machine Intelligence* **18**, pp. 279–292, March 1996.
4. E. Trucco, M. Umasuthan, A.M. Wallace and V. Roberto, "Model-based planning of optimal sensor placements for inspection," *IEEE Transactions on Robotics and Automation* **13**, pp. 182–194, April 1997.
5. F. Prieto, H.T. Redarce, P. Boulanger and R. Lepage, "CAD-based range sensor placement for optimum 3D data acquisition," in *Second International Conference on 3-D Digital Imaging and Modeling (3DIM'99)*, pp. 128–137, (Ottawa, Canada), 4-8 October 1999.
6. V. Moron, P. Boulanger, P. Masuda and H.T. Redarce, "Automatic inspection of industrial parts using 3-D optical range sensor," in *SPIE Proceedings, Videometrics IV*, vol. 2598, pp. 315–325, 1995.
7. P.J. Besl and N.D. McKay, "A method for registration of 3-D shapes," *IEEE Transactions on Pattern Analysis and Machine Intelligence* **14**, pp. 239–256, February 1992.
8. E.M. Bispo and R.B. Fisher, "Inspection of free-form surfaces using dense range data," in *SPIE Automated 3D and 2D Vision*, vol. 2249, pp. 211–220, (Frankfurt), June 1994.
9. T.S. Newman and A.K. Jain, "A system for 3D CAD-based inspection using range images," *Pattern Recognition* **28**(10), pp. 1555–1574, 1995.
10. F. Prieto, H.T. Redarce, R. Lepage and P. Boulanger, "Visual System for Fast and Automated Inspection of 3D Parts," *International Journal of CADCAM and Computer Graphics* **13**(4-5-6), pp. 211–227, 1998.
11. F. Prieto, H.T. Redarce, R. Lepage and P. Boulanger, "A non contact CAD based inspection system," in *Quality Control by Artificial Vision*, pp. 133–138, (Trois Rivières, Québec, Canada), 18-21 May 1999.
12. T. Masuda and N. Yokoya, "A robust method for registration and segmentation of multiple range images," *Computer Vision and Image Understanding* **61**(3), pp. 295–307, 1995.
13. V. Moron, P. Boulanger, H.T. Redarce, and A. Jutard, "Mise en correspondance du modèle CAO d'un objet avec son image 3D: Application à l'inspection," in *RIFIA'96, Congrès de Reconnaissances de Formes et Intelligence Artificielle*, pp. 913–922, (Rennes, France), 16-18 Janvier 1996.
14. P. Boulanger, *Extraction multiéchelle d'éléments géométriques.* Ph.D. Dissertation: Génie Electrique, Université de Montreal, Canada, 1994.